

Coupling and Propagation of Sommerfeld Waves at 100 and 300 GHz

Laurent Chusseau · Jean-Paul Guillet

Received: 8 September 2011 / Accepted: 24 October 2011 /
Published online: 11 November 2011
© Springer Science+Business Media, LLC 2011

Abstract The coupling between a linearly-polarized gaussian beam and a Sommerfeld wave propagating on a circular metallic wire is obtained owing to a differential phase element inserted in front of the metal wire. At millimeter-wavelengths we calculate a theoretical maximum coupling efficiency of 32% for this system in spite of the metal nature and radius in the range of a few hundreds of microns. A detailed experimental study of 100 and 300 GHz Sommerfeld waves propagating on stainless steel and tungsten wires is reported. The measured field at any distance from the wire compares well with theoretical predictions.

Keywords Far infrared · Waveguides · Surface plasmons

1 Introduction

The development of terahertz technology requires, besides the sources and the detectors, new components to handle beams appropriate to applications [1]. As is the case in the microwave and optical frequency ranges, waveguiding technology is expected to be the most convenient way to distribute and split signals between sources and detectors. The terahertz frequency range being intermediate between the microwave and optics frequency ranges, one may employ either dielectric or metallic waveguides. It seems that planar dielectric waveguides [2], dielectric fibers [3, 4], pipe waveguides [5], hollow glass waveguides [6], or polymer tube [7] are not as frequently employed

L. Chusseau (✉) · J.-P. Guillet
Institut d'Électronique du Sud, UMR 5214 CNRS, Université Montpellier 2,
Place E. Bataillon, 34095 Montpellier, France
e-mail: chusseau@univ-montp2.fr

than metallic waveguides. The latter are simply scaled down versions of classical waveguides, for example rectangular waveguides [8], circular waveguides [9], two-wire waveguide [10], or slit waveguides [11]. One may also employ structures that are more specific to the THz frequency range like parallel plate waveguides [12, 13], or the plasmonic metallic wire supporting cylindrical waves, studied by Goubau in the microwave frequency range [14], and recently shown to be of tremendous importance in the THz regime [15–25].

In this paper we study the propagation of cylindrical waves on metallic wires at 100 and 300 GHz. An original set up is described which helps us to evaluate the propagating field extension around the wire. We consider the coupling of linearly-polarized beams to such guided modes, and measure the propagating loss due to the metal non-zero resistivity. Comparison between our experimental results and theory is made.

2 Sommerfeld Waves

Electromagnetic waves guided by cylindrical metallic surfaces were described in [26]. Let z denote the metallic wire axial coordinate and let us employ cylindrical coordinates. Only the components E_z , E_r and H_φ do not vanish. For frequencies in the THz range and the usual ohmic losses the most important field component is the radial electric field E_r . It propagates in the air (or vacuum) surrounding the wire. We have $E_r \propto j_\gamma^h H_1^{(1)}(\gamma r) \exp^{j(\omega t - hz)}$, with $H_1^{(1)}$ the Hankel function of the first kind, h the propagation constant of the guided wave and $\gamma^2 = k^2 - h^2$ where k denotes the wavenumber in air. Its magnetic counterpart $H_\varphi = \omega \epsilon_0 E_r / h$. The small longitudinal electric field component $E_z \propto H_0^{(1)}(\gamma r) \exp^{j(\omega t - hz)}$ usually does not exceed a few percent of E_r [27]. The propagation constant h follows from the transcendental equation that derives from the continuity of the E_z component at the wire surface [14, 26]

$$\mu \frac{\gamma}{k^2} \frac{H_0^{(1)}(\gamma a)}{H_1^{(1)}(\gamma a)} = \mu_m \frac{\gamma_m}{k_m^2} \frac{J_0(\gamma_m a)}{J_1(\gamma_m a)} \tag{1}$$

where a is the wire radius, $\gamma_m^2 = k_m^2 - h^2$, and k_m is the wavenumber in the metal. μ_m / μ is the metal relative permeability that are always taken to 1 in this work. $H_0^{(1)}(\cdot)$ and $H_1^{(1)}(\cdot)$ are Hankel functions and $J_0(\cdot)$ and $J_1(\cdot)$ are Bessel functions of the first kind.

Equation 1 (or its dual form using the $I_n(\cdot)$ and $K_n(\cdot)$ generalized Bessel functions [27, 28]) cannot be solved in terms of known functions. Most solutions found in the literature characterize the metal only by its dc conductivity [14] and assume that the wire radius is large compared with the skin depth [14, 19]. Asymptotic expressions of the Bessel functions [27] or Taylor series expansions are used to obtain approximate solutions [28]. Here we directly solve Eq. 1 using arbitrary precision numerical facilities of Mathematica [29]. When pure metals are considered the Drude approximation of the permittivity is used because of its accuracy in the far infrared and THz frequency range

[30, 31]. Otherwise we use the permittivity derived from the Ohm law, $\epsilon = \epsilon_0 - j\sigma/\omega$, with ϵ_0 the vacuum permittivity and σ the dc conductivity. This procedure does not suffer from numerical approximations and is easy to implement. The main features of the waves sketched in [27] are accurately described by the present exact calculations. Namely, the large field extension outside the wire, a quasi TEM behavior in air, a phase velocity very close to the light speed c , and very low propagation losses due to the small penetration of the fields into metals.

3 Coupling Between Linearly-polarized Gaussian Beams and Sommerfeld Waves

The major difficulty when dealing with Sommerfeld waves is the low coupling efficiency between the wire and the usual sources. The main reason is the large difference between the radial polarization of wire modes and the usual sources generating linearly-polarized beams propagating in free-space. The first demonstrations of Sommerfeld waves employed an adiabatic transformation of coaxial modes [14, 32]. This technique is efficient and almost lossless but is practical only for microwave sources. With the renewed interest in Sommerfeld waves for the THz range, the concern has been mostly to couple to it the broadband impulse signals produced by photoconductive antennas. Mode matching has been obtained by various methods: concentrating a freely-propagating THz pulse using circular plasmonic grooves surrounding a circular aperture with a wire at its center [33], modifying the photoconductive cell itself so as to exhibit a radial symmetry [17, 34], exciting only one side of the wire with the near-field of a linearly polarized source [35], or using another metal wire to serve as an intermediate antenna breaking the radial symmetry at the focus point of a linearly polarized source (dual-wire coupler) [15, 16]. All these solutions operate well but with coupling efficiencies ranging from 0.4% for the dual-wire coupler to more than 50% with dedicated radial photoconductors [34]. Although highly satisfactory, the latter solution is restricted to photoconductive switches and thus cannot be adapted to other sources like quantum cascade lasers or frequency-multiplied microwave sources.

To solve the free-space to Sommerfeld mode coupling problem in the cw case, we previously proposed the use of a differential phase plate that induces a polarization reversal of one half-space as compared to the other before launching the electromagnetic field on the wire [36]. This is a direct translation of common practices in optics and its implementation to the THz range is schematically drawn in Fig. 1a.

The peculiarities of the Sommerfeld waves recalled earlier are that the propagating-wave phase velocity is close to c and that the reflection from wire ends is negligible [27]. Besides, the very small longitudinal (axial) electrical field renders the local field in air similar to a TEM wave. Since we are interested only in the coupling of the wire mode with an x -polarized input beam (such as an x -polarized gaussian beam with a half-space phase reversal)

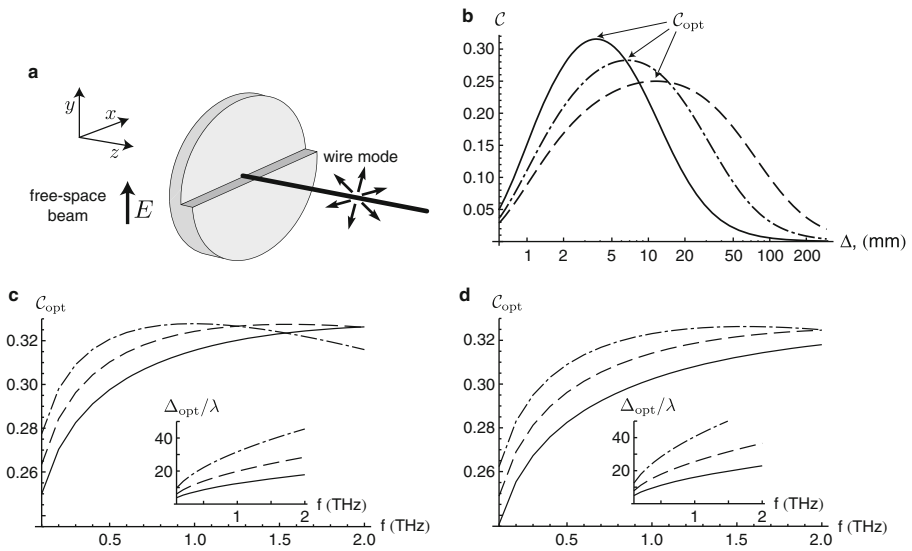


Fig. 1 Calculated coupling efficiency C between a linearly polarized gaussian beam of full-width at half power Δ and a Sommerfeld mode propagating along a metal wire of radius a . **(a)** Schematic of the coupling scheme. **(b)** Coupling to a tungsten wire of radius $a = 250 \mu\text{m}$ versus Δ : $f = 100 \text{ GHz}$, dashed line; $f = 300 \text{ GHz}$, dot-dashed line; $f = 1,000 \text{ GHz}$, solid line. **(c)** Tungsten and **(d)** Gold: Maximum coupling efficiency, C_{opt} , as a function of frequency for various wire radius: $a = 250 \mu\text{m}$, solid line; $a = 500 \mu\text{m}$, dashed line; $a = 1 \text{ mm}$, dot-dashed line. Insets give the ratio of Δ_{opt} to the wavelength, Δ_{opt} being the beam width that achieves the maximum coupling efficiency C_{opt} .

we may express the wire field in terms of a real field $\psi_B(x, y) = \cos(\theta)E_r(r)$ with $r = \sqrt{x^2 + y^2}$, $\tan(\theta) = y/x$, where: $E_r(r) = h H_1^{(1)}(\gamma r)/\gamma$, leaving aside normalization. The power coupling is [37]

$$C = \left(\int_S \psi_A \psi_B \, dS \right)^2. \tag{2}$$

where ψ_A represents the incident beam.

We evaluate C analytically for an incident gaussian field at its waist: $\psi_A(x, y) = \exp(-(x^2 + y^2)/(2\sigma^2))$. After the phase plate, we have: $\psi_A = \exp(-(x^2 + y^2)/(2\sigma^2))$, $y > 0$, $\psi_A = -\exp(-(x^2 + y^2)/(2\sigma^2))$, $y < 0$. Inserting ψ_A and ψ_B in Eq. 2 yields the power coupling.

First, we have calculated the power coupling defined above for various metals and parameters. Figure 1b gives calculated values of C as a function of $\Delta \equiv 2.35 \sigma$, which is approximately the full width at half maximum (FWHM) of the gaussian beam. A tungsten wire of radius $a = 250 \mu\text{m}$ and three frequencies were considered. As shown, C may exceed 30% when the input gaussian beam width is appropriately chosen. This occurs for beam sizes of a few millimeters, which are easily generated using off-axis parabolic mirrors. Moreover, the tolerance associated to these widths is great since more than

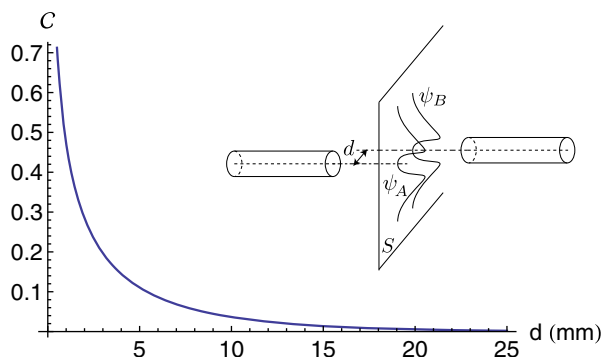
80% of the maximum coupling efficiency is obtained over a decade in Δ -values for the three frequencies considered.

Next, we investigate the influence of frequency and of the kind of metal employed on the maximum available coupling C_{opt} . This is illustrated in Fig. 1c and d by plots of C_{opt} versus frequency deduced from series of curves like that of Fig. 1b. Results are given for three different wire radii, $a = 250 \mu\text{m}$, $500 \mu\text{m}$ and 1 mm . Data in Fig. 1c relate to tungsten while those of Fig. 1d relate to gold. For each plot an inset shows the beam width Δ_{opt} corresponding to C_{opt} . The main conclusion is that the maximum coupling efficiency can be optimized up to $\approx 32\%$ at any frequency in the range considered provided that the wire radius is properly selected. The lower the frequency, the wider the radius a should be to optimize the coupling. Only a slight difference occurs in Δ_{opt} (see insets). The explanation is that the increase in the Sommerfeld mode extension as a function of a requires an increase of Δ to keep the coupling at its optimum value. Finally, a comparison between the results in Fig. 1c and d shows a similar behavior for other metals, even for very different conductivities. For similar conductivities (aluminum and gold), separate calculations show plots that are indistinguishable at the scale of Fig. 1d.

The analytic evaluation of the efficiency of the coupling scheme given in Fig. 1a thus predicts a power-coupling efficiency exceeding 30% whatever the frequency in the range considered and for the metals considered. This is achieved through an uncritical selection of the incident beam size. The C -values obtained here are close to the maximum limit of 50% that one would ideally obtain while projecting a linearly polarized gaussian mode with a half-space phase reversal on a radially polarized gaussian mode. As a consequence the additional $\approx 20\%$ loss calculated here most likely originates from wavefront mismatch.

The method involved in Eq. 2 is also suitable to calculate the coupling between two distinct metal wires separated a distance d apart. This situation is described in the inset of Fig. 2 and corresponds to $\psi_A(x, y) = h H_1^{(1)}(\gamma r)/\gamma$ and $\psi_B(x, y) = h H_1^{(1)}(\gamma r')/\gamma$ with $r = \sqrt{x^2 + y^2}$ and $r' = \sqrt{(x+d)^2 + y^2}$. We have calculated C at $f = 100 \text{ GHz}$ numerically in the case of tungsten wires of radius

Fig. 2 Calculated coupling efficiency C between the ends of two tungsten wires of radius $a = 250 \mu\text{m}$ supporting Sommerfeld propagating modes at $f = 100 \text{ GHz}$ and separated laterally by the distance d . The inset gives a schematic description of the system considered.



$a = 250 \mu\text{m}$ assuming the two wire ends close enough so that it is unnecessary to account for free-space propagation [36, 38]. The result given in Fig. 2 shows a rapid fall out of the coupled intensity as a function of d . As an example, when $d = 2a$ (the first point in Fig. 2) a drop of 25% of the transmission is obtained. This calculation explains quantitatively well the experiment described in [36] where the coupling between two such wires was shown to exhibit a FWHM $\approx \pm 2 \text{ mm}$.

4 Propagation of Sommerfeld Waves

With continuous-wave frequency-multiplied electronic sources, and the previously designed coupler, a preliminary experiment was conducted to verify that the propagating mode is a true Sommerfeld mode and to evaluate the radial extension of the field around the wire. This kind of experiment has already been performed in pulsed mode with a direct field detection by a photoconductive antenna [16, 17]. A good agreement with the known field profile has been found except for a reduced accuracy far from the metal wire. On the other hand, the field emission (radiation pattern) from the wire end has been measured [36, 38, 39]. It resembles the emission of traveling wave broadband antennas [40].

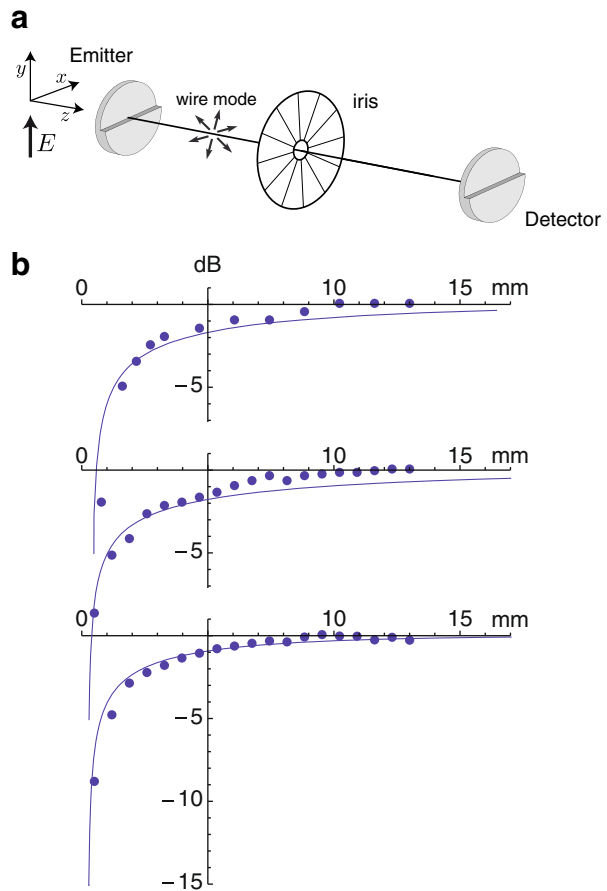
We propose here another kind of experiment involving an iris diaphragm of variable clear aperture around the metal wire supporting the Sommerfeld mode. By closing the iris the open space around the wire gets reduced and the mode transmission decreases (see Fig. 3a). As a major consequence, the power transmission of the system is reduced and easily measured. The experiment was conducted with various wires of length $\approx 20 \text{ cm}$ at two different frequencies. At 100 GHz the detection was obtained with a Schottky diode and at 300 GHz a 4K Si-bolometer was employed. Results are given as dots in Fig. 3b and show very similar behavior whatever the frequency and the metal. Attenuations of $\approx 10 \text{ dB}$ are observed when the iris is nearly completely closed and in contact with the wire. The transmitted power increases rapidly when the diaphragm is opened progressively. A nearly complete transmission is achieved at full opening. The propagating modes are experimentally found to be confined to cylinder volumes of radii between $5 \times a$ and $9 \times a$, depending on the frequency and wire radii.

Using the known theoretical field from Section 2, the experimental results can be compared to the calculated transmitted power obtained by

$$\mathcal{P}(r) = \int_a^r E_r H_\varphi 2\pi r \, dr \propto \int_a^r 2\pi r |E_r(r)|^2 \, dr \tag{3}$$

where the field inside the metal and the E_z component in air have been neglected. Data of Fig. 3 are plotted with the theoretical attenuations $\mathcal{P}(r)/\mathcal{P}(\infty)$, the propagation constant h having been previously determined by Eq. 1 for the $a = 250 \mu\text{m}$ tungsten wire and the $a = 400 \mu\text{m}$ stainless steel wire of bulk resistivity $1.32 \cdot 10^6 \Omega^{-1}\text{m}^{-1}$. Comparisons between measurements and

Fig. 3 (a) Schematic of the transmission experiment of a Sommerfeld mode on a wire of radius a with an iris as a variable attenuator. (b) Measured (dots) and calculated (solid lines) power transmissions as a function of the iris opening radius. Abscissa origin is taken at the wire center. *Upper curve:* stainless steel $a = 400 \mu\text{m}$ $f = 100 \text{ GHz}$. *Middle curve:* tungsten $a = 250 \mu\text{m}$ $f = 100 \text{ GHz}$. *Lower curve:* tungsten $a = 250 \mu\text{m}$ $f = 300 \text{ GHz}$.



calculations are in excellent agreement on the whole range of the diaphragm opening. Calculations also show that the modes are more confined at higher frequency and that the metal nature has little influence provided that the conductivity is high. These features are known to scale down up to the μm size [21, 22, 41], thus allowing a high field concentration at the wire end that can serve as an excellent near-field probe mostly sensitive to the longitudinal E_z component [25]. The perfect agreement between measurement and theory shows that Sommerfeld waves are indeed excited and that propagation lengths of $\approx 20 \text{ cm}$ prohibit the propagation of other low-loss mode.

Using the same experimental setup and with the iris diagram fully opened, the propagation losses are easily estimated by reducing step by step the wire length at the detection side. We already proposed this procedure [25] for wire lengths decreasing from 65 to 40 cm but the previously estimated losses were unexpectedly high. Our new experiments at $f = 100 \text{ GHz}$ give losses of $0.13 \pm 0.02 \text{ dB cm}^{-1}$. Measured results are however still high as compared to other measured data [15, 18]. They are estimated to be about three times larger

than the calculated value 0.043 dB cm^{-1} . A similar discrepancy was found in the earliest loss measurements of wire modes [32] and attributed to radiation losses at surface imperfections. Because of the excellent surface aspect of the wire used, we believe that the wire sag under its weight is the cause of the excess losses. A large, unobservable, radius of curvature of the wire was unavoidable during our experiments. This may have resulted into bending or mismatch losses being added to linear losses.

As a consequence, from the full balance of power in the experiment (i. e. 18 dB of attenuation with the two couplers and a 40 cm steel wire) one deduces a revised experimental efficiency of $23 \pm 2\%$ per coupler in reasonably good agreement with previous theoretical estimates. Discrepancy is attributed to the imperfect size matching of the gaussian input beam, and to a possible misalignment between that beam and the wire axis that was not controlled with precision.

5 Conclusion

We have efficiently coupled and propagated continuous-wave Sommerfeld modes on various metallic wires at millimeter-wavelengths. Using the theoretical form of the electric field guided along the wire, we have calculated a 32% optimum cw coupling efficiency with a simple differential phase element inserted in front of the metallic wire. Efficiencies exceeding 30% are theoretically obtained irrespectively of the metals investigated from a proper selection of the input gaussian beam waist. From the known experimental propagation losses we deduced a 23% coupling efficiency in experimental conditions. This result is in reasonably good agreement with calculations since no special care was taken to match the input gaussian beam size. With a simple set-up involving an iris surrounding the metal wire, propagating modes are shown experimentally to be in very good agreement with their known theoretical form, emphasizing that only this mode is guided along the wire.

Acknowledgements The authors acknowledge the French National Research Agency for funding under grant TERASCOPE, #ANR-06-BLAN-0073. Authors are also highly grateful to Jacques Arnaud for fruitful discussions and careful reading of the manuscript.

References

1. M. Tonouchi, *Nature Photonics* **1** 97 (2007).
2. R. Mendis and D. Grischkowsky, *Journal of Applied Physics* **88**, 4449 (2000).
3. L.-J. Chen, H.-W. Chen, T.-F. Kao, J.-Y. Lu, and C.-K. Sun, *Optics Letters* **31**, 308 (2006).
4. C. Jördens, K. L. Chee, I. A. I. Al-Naib, I. Pupeza, S. Peik, G. Wenke, and M. Koch, *J. Infrared Millim. Terahertz Waves* **31**, 214 (2010).
5. C.-H. Lai, Y.-C. Hsueh, H.-W. Chen, Y.-J. Huang, H.-C. Chang, and C.-K. Sun, *Opt. Lett.* **34**, 3457 (2009).
6. B. Bowden, J. A. Harrington, and O. Mitrofanov, *Opt. Lett.* **32**, 2945 (2007).
7. D. Chen and H. Chen, *Opt. Express* **18**, 3762 (2010).

8. D. Grischkowsky, *IEEE Journal of Selected Topics In Quantum Electronics* **6**, 1122 (2000).
9. G. Gallot, S. P. Jamison, R. W. McGowan, and D. Grischkowsky, *J. Opt. Soc. Am. B* **17**, 851 (2000).
10. M. Mbonye, R. Mendis, and D. M. Mittleman, *Applied Physics Letters* **95**, 233506 (2009).
11. M. Wächter, M. Nagel, and H. Kurz, *Appl. Phys. Lett.* **92**, 161102 (2008).
12. S.-H. Kim, E. S. Lee, Y. B. Ji, and T.-I. Jeon, *Opt. Express* **18**, 1289 (2010).
13. H. Zhan, R. Mendis, and D. M. Mittleman, *Optics Express* **18**, 9643 (2010).
14. G. Goubau, *J. Appl. Phys.* **21**, 1119 (1950).
15. K. Wang and D. Mittleman, *Nature* **432**, 376 (2004).
16. K. Wang and D. Mittleman, *J. Opt. Soc. Am. B* **22**, 2001 (2005).
17. T. Jeon, J. Zhang, and D. Grischkowsky, *Appl. Phys. Lett.* **86**, 161904 (2005).
18. M. Wächter, M. Nagel, and H. Kurz, *Optics Express* **13**, 10815 (2005).
19. K. Wang and D. Mittleman, *Phys. Rev. Lett.* **96**, 157401 (2006).
20. T. Akalin, A. Treizebre, and B. Bocquet, *IEEE Trans. Microwave Theo. Techn.* **54**, 2762 (2006).
21. Y. B. Ji, E. S. Lee, J. S. Jang, and T.-I. Jeon, *Opt. Express* **16**, 271 (2008).
22. X.-Y. He, *J. Opt. Soc. Am. B* **26**, A23 (2009).
23. M. Awad, M. Nagel, and H. Kurz, *Appl. Phys. Lett.* **94**, 051107 (2009).
24. V. Astley, J. Scheiman, R. Mendis, and D. M. Mittleman, *Opt. Lett.* **35**, 553 (2010).
25. J.-P. Guillet, L. Chusseau, R. Adam, T. Grosjean, A. Penarier, F. Baida, and D. Charrat, *Microwave and Optical Technology Letters* **53**, 580 (2011).
26. A. Sommerfeld, *Electrodynamics* (Academic Press, New York, 1952).
27. Q. Cao and J. Jahns, *Opt. Express* **13**, 511 (2005).
28. J. Yang, Q. Cao, and C. Zhou, *Optics Express* **17**, 20806 (2009).
29. *Mathematica 8*, Wolfram Research Inc. (2011), <http://www.wolfram.com/mathematica/>.
30. M. A. Ordal, R. J. Bell, R. W. Alexander, L. L. Long, and M. R. Querry, *Applied Optics* **24**, 4493 (1985).
31. M. A. Ordal, R. J. Bell, R. W. Alexander, L. A. Newquist, and M. R. Querry, *Applied Optics* **27**, 1203 (1988).
32. F. Sobel, F. L. Wentworth, and J. C. Wiltse, *IRE Trans. Microwave Theory Tech.* **9**, 512 (1961).
33. A. Agrawal and A. Nahata, *Opt. Express* **15**, 9022 (2007).
34. J. Deibel, K. Wang, M. Escarra, and D. Mittleman, *Opt. Express* **14**, 279 (2006).
35. M. Walther, M. Freeman, and F. Hegmann, *Appl. Phys. Lett.* **87**, 261107 (2005).
36. R. Adam, L. Chusseau, T. Grosjean, A. Penarier, J.-P. Guillet, and D. Charrat, *Journal of Applied Physics* **106**, 073107 (2009).
37. J. A. Arnaud, *Beam and Fiber Optics* (Academic Press, 1976).
38. J. A. Deibel, N. Berndsen, K. Wang, D. M. Mittleman, N. C. J. van der Valk, and P. C. M. Planken, *Opt. Express* **14**, 8772 (2006).
39. M. Walther, G. S. Chambers, Z. G. Liu, M. R. Freeman, and F. A. Hegmann, *J. Opt. Soc. Am. B* **22**, 2357 (2005).
40. C. A. Balanis, *Antenna Theory - Analysis and Design* (John Wiley & Sons Inc., 1982), 2nd ed.
41. H. Liang, S. Ruan, and M. Zhang, *Opt. Express* **16**, 18241 (2008).